ARTICLES
https://doi.org/10.1038/s41565-022-01179-0
nature nanotechnology

Check for updates

Nanozyme-catalysed CRISPR assay for preamplification-free detection of non-coding RNAs

Marta Broto[1,11], Michael M. Kaminski[2,3,4,11], Christopher Adrianus[1,11], Nayoung Kim[1], Robert Greensmith[2,3], Schan Dissanayake-Perera[1], Alexander J. Schubert[2,3,4], Xiao Tan[5,6,7,8], Hyemin Kim[1], Anand S. Dighe[7,9], James J. Collins[5,8,10] ✉ and Molly M. Stevens[1] ✉

CRISPR-based diagnostics enable specific sensing of DNA and RNA biomarkers associated with human diseases. This is achieved through the binding of guide RNAs to a complementary sequence that activates Cas enzymes to cleave reporter molecules. Currently, most CRISPR-based diagnostics rely on target preamplification to reach sufficient sensitivity for clinical applications. This limits quantification capability and adds complexity to the reaction chemistry. Here we show the combination of a CRISPR–Cas-based reaction with a nanozyme-linked immunosorbent assay, which allows for the quantitative and colorimetric readout of Cas13-mediated RNA detection through catalytic metallic nanoparticles at room temperature (CrisprZyme). We demonstrate that CrisprZyme is easily adaptable to a lateral-flow-based readout and different Cas enzymes and enables the sensing of non-coding RNAs including microRNAs, long non-coding RNAs and circular RNAs. We utilize this platform to identify patients with acute myocardial infarction and to monitor cellular differentiation in vitro and in tissue biopsies from prostate cancer patients. We anticipate that CrisprZyme will serve as a universally applicable signal catalyst for CRISPR-based diagnostics, which will expand the spectrum of targets for preamplification-free, quantitative detection.

Clustered regularly interspaced short palindromic repeats (CRISPR) systems and CRISPR-associated (Cas) enzymes function as an adaptive immune system in microbes and have been repurposed as diagnostic technologies in recent years[1–4]. Here sensing of DNA or RNA is mediated through a complementary guide RNA (gRNA), which induces the activation of a Cas enzyme that indicates the presence of a target analyte. To this end, a wide variety of assays have been reported which differ in the usage of different Cas enzymes, reporter molecules or readout technologies. These assays have enabled the sensitive and specific detection of a wide range of pathogens[5], various biomarkers of human disease[6,7] and genetic variants[2,8], and have even been applied to the sensing of small molecules or proteins[9].

However, most current CRISPR-based diagnostic methods rely on the preamplification of the target upstream of the CRISPR reaction. To this end, polymerase chain reaction (PCR)[10] or isothermal amplification methods[8] are commonly used. While these primer-based amplification techniques enable the detection of single DNA or RNA molecules in a reaction, PCR requires thermal cycling which limits its use as a point-of-care diagnostic, and isothermal amplification can suffer from complex primer design[8,11], non-specific amplification[12] and challenging quantification[3]. Moreover, the detection of specific mutations or sensing of very short target sequences, such as microRNAs (miRNAs), can restrict the design flexibility of an optimal gRNA, which requires methods for signal amplification. In addition, there is a critical need for versatile CRISPR diagnostics that are easily adaptable to point-of-care readouts, work at ambient temperature and allow for usage with different Cas enzymes. Thereby, they could fully exploit the ease of use and programmability of this technology and enable quantitative sensing in resource-limited settings.

Here we report the development of CrisprZyme, the combination of a Cas-based reaction with a nanozyme-linked immunosorbent assay (NLISA) (Fig. 1). NLISA serves as a signal catalyst of reporter RNA detection; it is a stepwise addition of reagents onto an immobilized surface that ends with the catalysis of a substrate to generate a readout signal. The substrate conversion rate of nanozymes, which comprise nanometre-sized catalytic metallic particles, is higher than their enzymatic counterparts[13], thus making NLISA even more sensitive than enzyme-linked immunosorbent assays (ELISA). Furthermore, NLISA offers high-throughput capability and ease of use. We designed nanozymes that are immobilized through an RNA linker oligonucleotide and can catalyse the oxidation of a chromogenic substrate. In the presence of the RNA target analyte, the RNA linker oligonucleotide gets degraded through Cas13-mediated collateral cleavage resulting in the absence of a colour change. We validated CrisprZyme using synthetic standards and RNA isolated from cell lines, patient tissue biopsies and plasma. We further adapted the assay for a lateral-flow-based readout and combined CrisprZyme with different Cas13 enzymes for enhanced sensitivity.

Nanozyme functionalization and characterization

We selected bimetallic nanozymes composed of platinum and gold (Pt@Au) due to their high catalytic activity[13]. Briefly, Pt@Au

[1]Department of Materials, Department of Bioengineering, and Institute of Biomedical Engineering, Imperial College London, London, UK. [2]Berlin Institute for Medical Systems Biology, Max Delbrück Center for Molecular Medicine in the Helmholtz Association, Berlin, Germany. [3]Department of Nephrology and Medical Intensive Care, Charité Universitätsmedizin Berlin, Berlin, Germany. [4]Berlin Institute of Health, Berlin, Germany. [5]Wyss Institute for Biologically Inspired Engineering, Harvard University, Boston, MA, USA. [6]Division of Gastroenterology, Massachusetts General Hospital, Boston, MA, USA. [7]Harvard Medical School, Boston, MA, USA. [8]Institute for Medical Engineering and Science and Department of Biological Engineering, Massachusetts Institute of Technology, Cambridge, MA, USA. [9]Department of Pathology, Massachusetts General Hospital, Boston, MA, USA. [10]Infectious Disease and Microbiome Program, Broad Institute of MIT and Harvard, Cambridge, MA, USA. [11]These authors contributed equally: Marta Broto, Michael M. Kaminski, Christopher Adrianus. ✉e-mail: jimjc@mit.edu; m.stevens@imperial.ac.uk

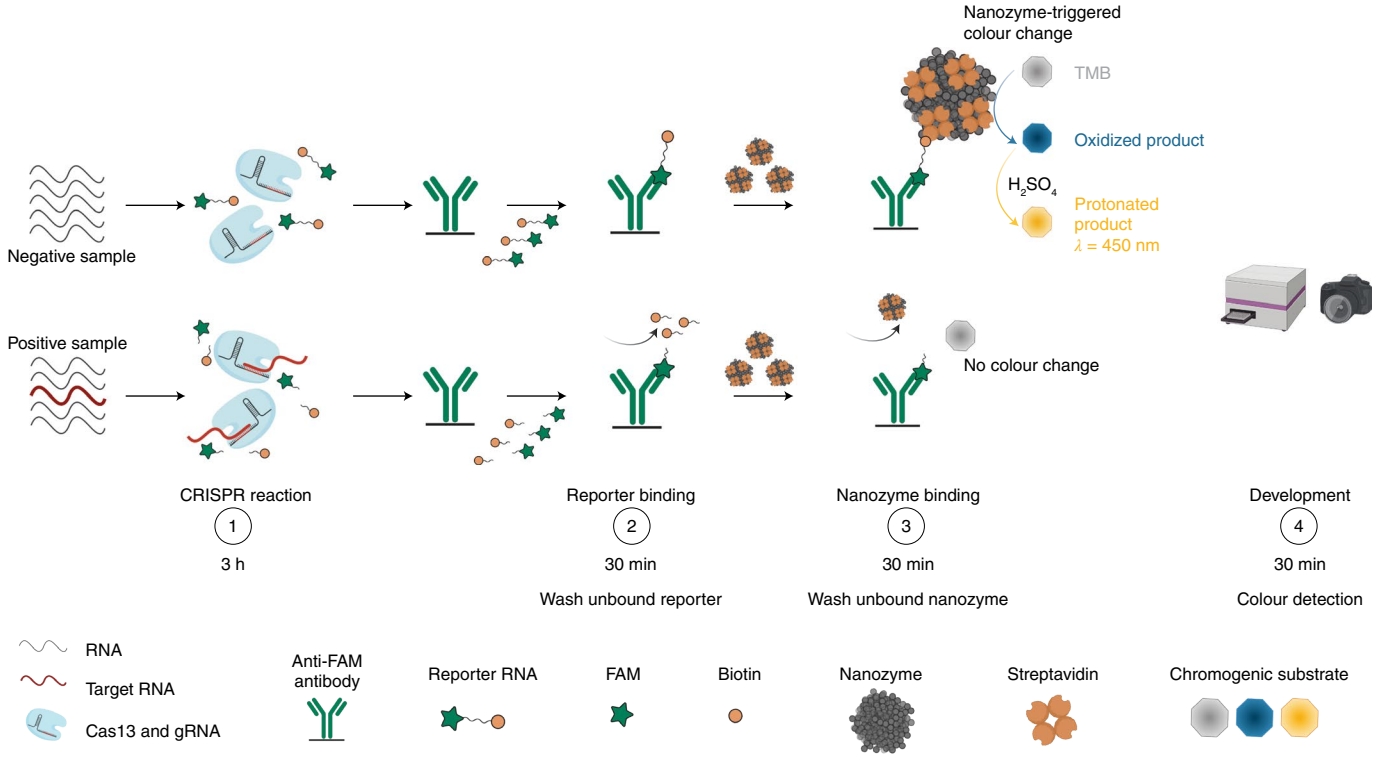

Fig. 1 | CrisprZyme assay scheme. Schematic of the combination of a Cas-based reaction with a NLISA proposed in this study. Target RNA is mixed with the gRNA–Cas13 complex and triggers collateral cleavage of reporter RNA. Subsequently, the mixture is added to an immunoassay plate precoated with anti-FAM. The unbound reporter RNA is washed away, and the nanozymes are added to form a complex through the bound reporter RNA. Finally, the substrate is added for colour development.

nanozymes were synthesized through a seed-mediated platinum overgrowth method using 15 nm gold nanoparticles as seeds, whereby polyvinylpyrrolidone (PVP) and L-ascorbic acid served as a stabilizer and a reducing agent for platinum, respectively[13] (Fig. 2a). Next, we functionalized Pt@Au particles with a biotin-binding protein to bind them to the biotinylated reporter RNA. First, we tested different functionalization procedures for optimal binding through the variation of pH, protein concentrations and blocking agents. We found that pH 6.4–6.5, slightly above the isoelectric point of the biotin-binding protein (5 and 6.3 for streptavidin and neutravidin, respectively), resulted in a higher signal-to-noise (S/N) ratio (Supplementary Fig. 1). This is because the slight positive charge of the protein interacts strongly with the negatively charged particles. Next, we aimed to improve the S/N ratio further by testing different biotin-binding proteins and blocking agents (Fig. 2b). From this, we selected a combination of streptavidin and phosphate-buffered saline solution containing 0.05% v/v Tween-20 (PBST) for higher S/N ratios. Protein blocking through addition of beta casein or bovine serum albumin (BSA) was not required to avoid non-specific interaction between the particles and proteins on the NLISA plate. The particles were characterized by dynamic light scattering (DLS) to determine the functionalized particle size. The functionalized particles were found to be highly monodisperse, with a polydispersity index below 0.074. Also, a ζ-potential change, from −44.3 mV to −25.6 mV, confirmed the presence of proteins on the surface of the particles.

To achieve the lowest limit of detection (LOD) of the reporter RNA concentration, calculated as EC_{10}, we tested the effect of nanozyme size. We first overgrew different amounts of Pt onto Au seeds to prepare particles with a range of diameters from 68 nm to 220 nm (Fig. 2c). Next, we performed a two-dimensional titration assay to select the best concentration of both anti-6-carboxyfluorescein antibody (anti-FAM) and streptavidin-Pt@Au. The objective of the titration assay was to obtain a single monolayer of anti-FAM on the plate, found when the signal of the titration reaches assay saturation, and to obtain an absorbance of ~1, selected arbitrarily outside the absorbance saturation range. We found 100 ng ml^{-1} of anti-FAM and 250 fM of streptavidin-Pt@Au to be the best combination (Supplementary Fig. 2). We then determined the optimal reporter RNA concentration, measured using these different particle sizes (Fig. 2d). We observed that a bigger particle size resulted in higher absorbance without compromising the LOD. Bigger particles enabled larger catalytic surface area per binding event, thereby increasing the detection capability. With this optimized assay design, using 188 nm particles, we achieved an LOD of 611 fM of reporter RNA. These optimized conditions were used in the experiments described below.

Transmission electron microscopy (TEM) and scanning transmission electron microscopy (STEM) bright-field images showed spherical nanoparticles of ~200 nm in diameter with nanometre-sized pores (~1–2 nm) throughout the surface (Fig. 2e and Supplementary Fig. 3). The nanoscale pores are selectively accessible to small molecules (for example, H_2O_2) and significantly increase the surface area for catalytic amplification, as we previously reported[13]. On the other hand, functionalizing with streptavidin did not induce any noticeable change in the overall morphology and size of Pt@Au. Notably, however, we observed that a thin layer of amorphous substance on the surface of Pt@Au had formed, which presumably indicates the successful functionalization of the protein layer on the surface (Supplementary Fig. 4). We performed high-angle annular dark-field STEM (HAADF-STEM) that shows the atomic number contrast and applied energy dispersive X-ray spectroscopy (EDS) to analyse the elemental distribution in Pt@Au and streptavidin-Pt@Au (Figs. 2f–g and Supplementary Fig. 5).

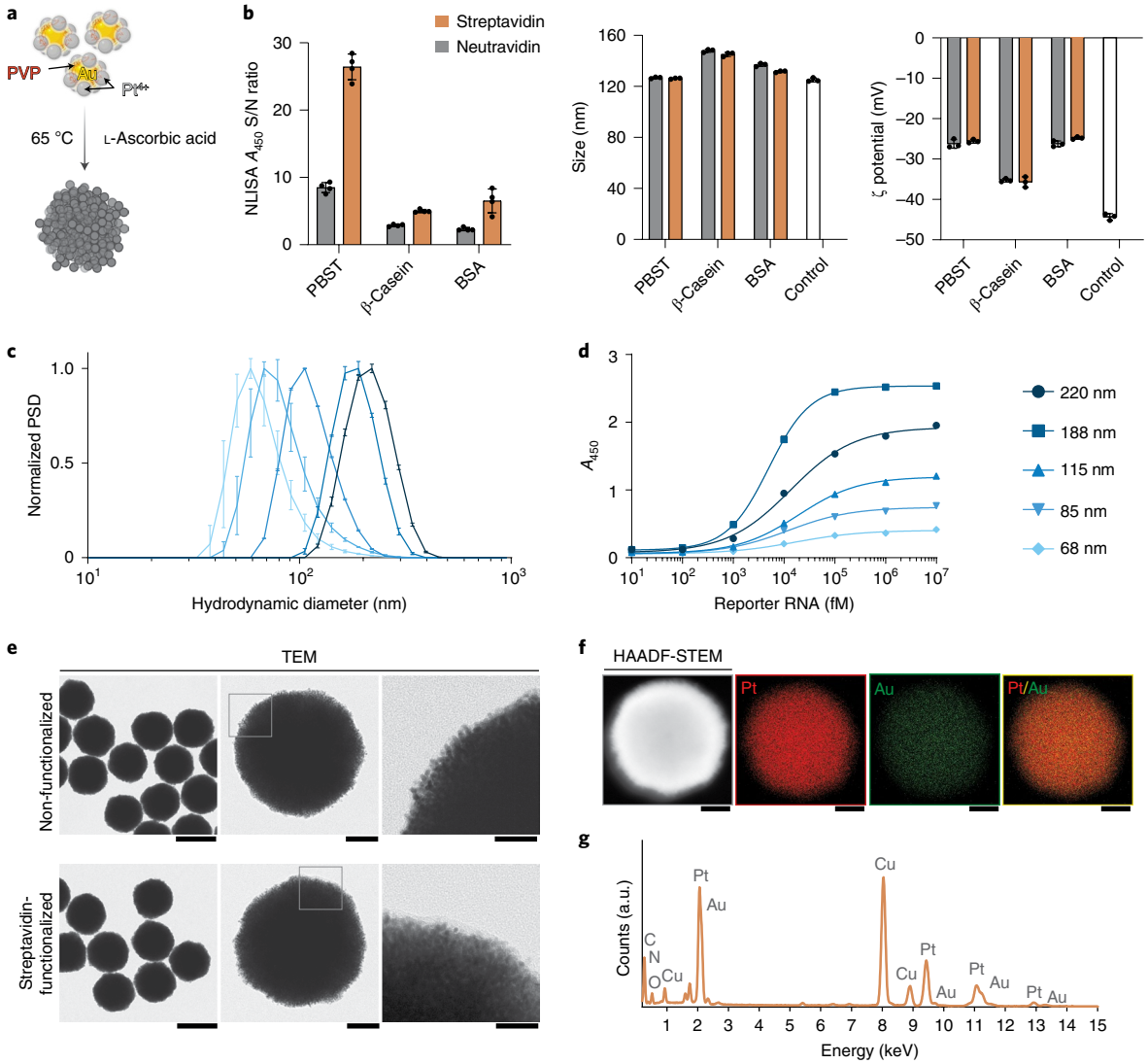

Fig. 2 | Pt@Au functionalized with streptavidin shows the best NLISA performance. a, Schematic showing the synthesis of Pt@Au. **b**, Characterization of the functionalized Pt@Au by S/N ratio and DLS with PBST and PBST supplemented with two different blocking agents: β-casein and BSA. Control corresponds to non-functionalized particles. Data points represent individual experiments. Error bars represent s.d. ($n > 3$ replicates). A_{450}, absorbance measure at 450 nm. **c**, Number distribution of the hydrodynamic diameter of the Pt@Au prepared by overgrowing different amounts of Pt onto the surface of AuNP seeds or 120 nm Pt@Au. Data represent the mean ± s.d. ($n = 3$ replicates). PSD, particle size distribution. **d**, Sigmoidal regression curve of the reporter RNA with streptavidin-Pt@Au of different sizes. Data represent the mean ($n = 2$ replicates). **e**, Structural characterization of non-functionalized and streptavidin-functionalized Pt@Au using TEM. Scale bars (from left to right), 200 nm, 50 nm and 20 nm. **f**,**g**, STEM–EDS analysis of streptavidin-functionalized Pt@Au. **f**, Representative HAADF-STEM image and EDS elemental mapping (Pt and Au). A merged image of Pt and Au maps is shown. Scale bar, 50 nm. **g**, Representative EDS spectra recorded from the whole area of the individual particle.

The EDS elemental maps and intensity point/line profile analyses revealed that Pt and Au were present throughout the inner particle while Pt was the main element found in the periphery region.

Optimization of the NLISA

Next, we incorporated the streptavidin-Pt@Au into the NLISA system. This assay consisted of four sequential steps: the addition of (1) antibodies directed against 6-carboxyfluorescein (anti-FAM), (2) the reporter RNA conjugated with a FAM and a biotin molecule at each end (5′-FAM-UUUUUC-biotin-3′), (3) streptavidin-functionalized nanoparticles (streptavidin-Pt@Au) and (4) finally the chromogenic substrate, 3,3′,5,5′-tetramethylbenzidine (TMB), for colour development. The chromogenic substrate is a colourless solution that becomes coloured with absorption maxima at 450 nm once protonated with a sulfuric acid solution. Between each of the described steps, an extra wash step is performed with washing buffer (PBST), except after addition of the chromogenic substrate. The complex formed between the anti-FAM and streptavidin-Pt@Au through the reporter RNA determines its concentration. In this study, we used a four-parameter sigmoidal regression curve to process the data as described in Supplementary equation (1).

RNA quantification using CrisprZyme

To develop a sensitive assay for the detection of target RNA, we next combined the NLISA quantification method with Cas13-based RNA detection (CrisprZyme, Fig. 1). For assay optimization, we used a synthetic 71-nucleotide RNA as target analyte. In brief, a master mix containing Cas13 from *Leptotrichia wadeii* (LwaCas13a), gRNA and reporter RNA was mixed with the target RNA to trigger the cleavage of the reporter RNA labelled with FAM

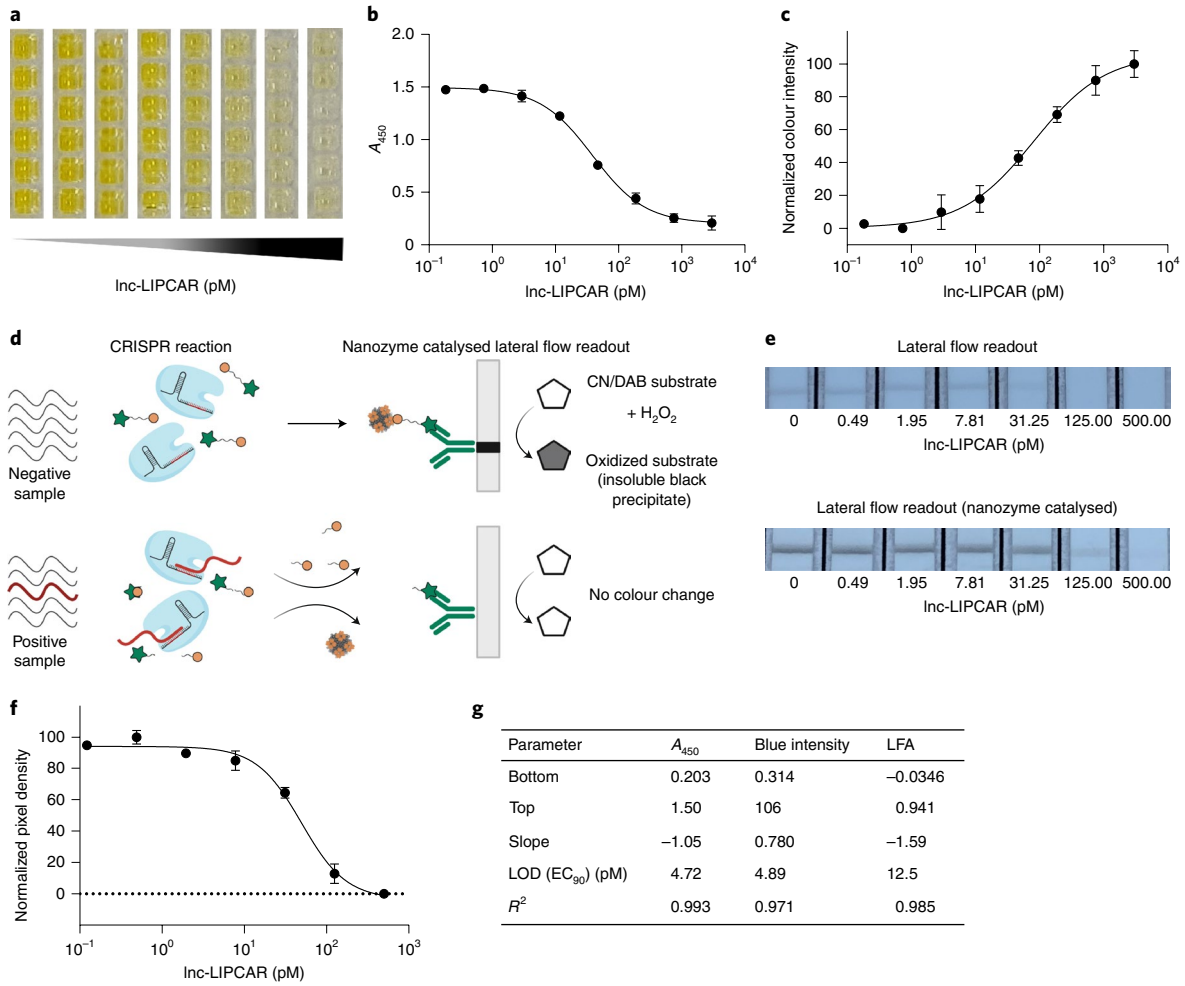

g

Parameter	A_{450}	Blue intensity	LFA
Bottom	0.203	0.314	–0.0346
Top	1.50	106	0.941
Slope	–1.05	0.780	–1.59
LOD (EC_{90}) (pM)	4.72	4.89	12.5
R^2	0.993	0.971	0.985

Fig. 3 | CrisprZyme detects synthetic RNA down to picomolar concentration. a, Photograph of CrisprZyme results in a 384-well plate; six replicates were performed for each concentration. Low concentration of a lncRNA target (lnc-LIPCAR) to the left; high concentration to the right. **b**, Sigmoidal regression of the CrisprZyme of a lncRNA target. Data were obtained measuring the absorbance of each well with a plate reader at 450 nm (A_{450}). **c**, Sigmoidal regression of the CrisprZyme of a lncRNA target. Data were obtained by taking a photo of the results and recording the blue intensity of each well set as a region of interest. **b**,**c**, Data represent the mean ± s.d. ($n = 6$ replicates). **d**, Schematic of the combination of a Cas-based reaction with a nanozyme-amplified LFA proposed in this study. Target RNA is mixed with the gRNA–Cas13 complex and reporter RNA to trigger the CRISPR reaction. Subsequently, streptavidin-functionalized nanozymes were mixed with CRISPR reaction product containing the biotinylated reporter RNA to form a complex. A test strip preprinted with anti-FAM was used to draw up the mixture. The uncleaved reporter RNA-nanozymes complexes were captured at the test line. Finally, the substrate was added for colour development. **e**, Detection of a serial dilution of lnc-LIPCAR with nanozyme-amplified LFA. Photographs show the test bands of the lateral flow test strips after completion of the assay without (top) and with (bottom) the substrate added for enhanced signal. **f**, Sigmoidal regression of the lnc-LIPCAR target for the nanozyme-amplified LFA. Data represent the mean of test line pixel density normalized to the internal grid lines of the light box. Data represent the mean ± s.d. ($n = 3$ replicates). **g**, Sigmoidal regression curve parameters. The data have been extracted from the four-parameter equation (Supplementary equation 1) used to fit the standard curve.

and biotin. The reaction product was then added to the NLISA to quantify the amount of cleaved reporter RNA. Cleavage of reporter RNA occurred in the presence of the target analyte, preventing the reporter RNA-mediated binding between the anti-FAM antibody and the streptavidin-functionalized nanozyme. The lack of binding reduces the linking of nanozyme particles, due to the removal of unbound particles during the wash step. This reduction in the number of particles resulted in a lower catalytic activity and less chromogenic substrate oxidation. The presence of the target analyte therefore inhibited colour development, whereas its absence increased the nanozyme-triggered colour change.

We first optimized the components of the reaction including buffers, enzyme and reporter concentrations (Supplementary Fig. 6). We observed that the reporter RNA concentration that showed the lowest LOD was 0.1 nM, which is more than two orders of magnitude lower than previously reported Cas13 assays[14]. We concluded that NLISA allowed for quantification of reporter RNA at lower concentrations than the fluorescent readout. Testing different ratios of gRNA to Cas13, we found a molar ratio of 1.2:1 (gRNA:Cas13) further increased sensitivity 10-fold. The optimized CrisprZyme assay allowed for the colour change that indicates different concentrations of target RNA to be observed by the naked eye (Fig. 3a). Quantification of the colour change with a plate reader showed a LOD of 4.72 pM through the measurement of absorbance at 450 nm (A_{450}) (Fig. 3b,g), while image analysis of the blue intensity in the central pixel of each well resulted in an LOD of 4.89 pM (Fig. 3c,g). Importantly, all LwaCas13a-based CrisprZyme assays were fully run at ambient temperature. Next, we adapted CrisprZyme for the readout with a lateral flow assay (LFA) (Fig. 3d). Target RNA is mixed with the gRNA–Cas13 complex and reporter RNA in the

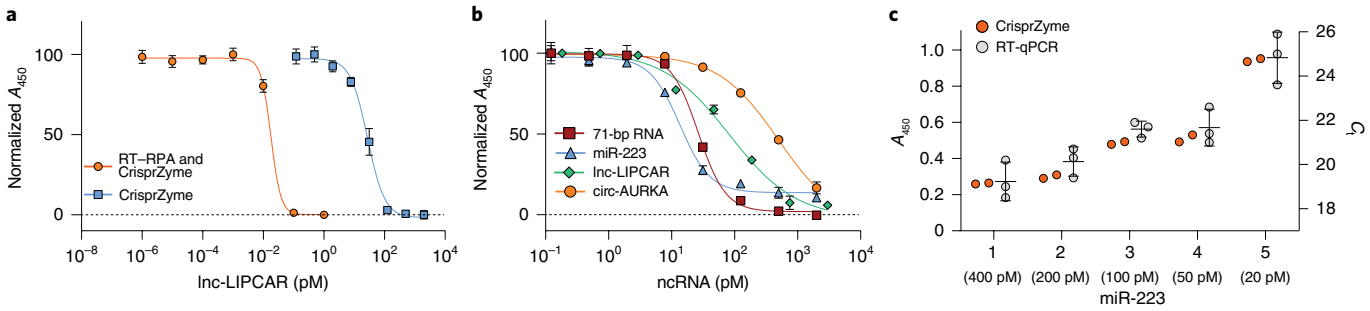

Fig. 4 | CrisprZyme expands the dynamic range of Cas13-based diagnostics enabling the quantitative sensing of different non-coding RNA species. **a**, Standard curves for the detection of serial dilutions of lnc-LIPCAR with CrisprZyme (blue) or a combination of RT–RPA and CrisprZyme (orange). Data represent the mean ± s.d. ($n = 6$ replicates). **b**, Comparison of the performance of CrisprZyme with different ncRNA targets: lnc-LIPCAR, miR-223, synthetic ncRNA (71-bp RNA) and circ-AURKA. Data represent the mean ± s.d. ($n \geq 3$ replicates). **c**, Detection of miR-223 with CrisprZyme (orange) or RT–qPCR (grey) in five different samples at the indicated concentrations. C_t, cycle threshold for PCR reactions. Data represent individual replicates ($n \geq 2$ replicates).

CRISPR reaction. Subsequently, streptavidin-functionalized nanozymes are mixed with the CRISPR reaction product containing the biotinylated reporter RNA to form a complex. A test strip composed of a nitrocellulose membrane and an absorbent pad was preprinted with anti-FAM and used to draw the mixture by capillary action. This allowed the capture of the non-cleaved reporter RNA–nanozyme complex on the test line. When exposed to the substrate solution, the nanozymes on the test line catalysed the substrate oxidation generating an insoluble black line. By quantifying the pixel density on the test line on the image taken using a smartphone (Fig. 3e), we achieved a LOD of 12.5 pM (Fig. 3f,g). It is noteworthy that β-casein blocking on the particles is required to minimize the non-specific binding of the LFAs.

To confirm the assay's simplicity, we next tested whether CrisprZyme could be run in both 96- and 384-well plates (Supplementary Fig. 7a), allowing for high-throughput applications. The presence of non-targeting RNA strands in the background RNA isolated from HEK293 T cells (Supplementary Fig. 7b) resulted in a decrease in sensitivity of one order of magnitude. The assay time of the nanozyme part of CrisprZyme was dependent on the readout technology ranging between 30 min for lateral flow to 90 min for the plate reader format (Supplementary Table 1). Combined with the Cas reaction (3 h) the total assay time was 3.5 h for lateral flow or 4.5 h for the plate reader. Further work should address shorter Cas reaction times followed by nanozyme-based readouts. Also, a full comparison of molecular diagnostic technology price (Supplementary Fig. 8) shows that our technology compares in consumable price to SHERLOCK and DETECTR strategies[2,15], without the requirement of purchasing small equipment such as a heatblock.

Expanding the dynamic range of Cas13-based diagnostics

To assess target RNA concentrations amenable for quantitative detection, we tested different Cas13-based assays for their dynamic range. The conventional fluorescence-based Cas13 assay achieved an LOD in the picomolar range which is consistent with previously reported results[16] (Supplementary Fig. 9). CrisprZyme showed an LOD of 7.88 ± 3.21 pM (Fig. 4a and Supplementary Table 2) and is comparable with other amplification-free strategies that require an electrochemical-powered readout[6]. Importantly, the LOD was similar when using lateral flow as readout or performing the reaction at room temperature underlining its potential for point-of-care applications. Furthermore, a shallow regression slope of −1.69 ± 0.30 would allow for the use of this technology in a quantitative format. Since various different Cas enzymes exist whose diverse properties can be leveraged for diagnostics, we next tested if CrisprZyme could be combined with LbuCas13a instead of LwaCas13a (Supplementary Fig. 10 and Supplementary Table 2). While the CRISPR reaction components need to be adapted to meet the requirements of LbuCas13a as previously described[17], the nanozyme-based readout did not require modifications underscoring its versatility. Importantly, LbuCas13a increased the LOD of the assay to the femtomolar range (264.2 ± 0.16 fM), which further extends the spectrum of potential target analytes.

To further evaluate CrisprZyme's versatility, we investigated the additive combination of CrisprZyme catalysis and a preamplification step as described in the SHERLOCK technology[2]. We included reverse transcription recombinase polymerase amplification (RT–RPA), followed by T7-based RNA transcription, Cas13 detection and NLISA. This enhanced the sensitivity to an LOD of 8.30 ± 0.97 fM (Fig. 4a and Supplementary Table 2). However, due to exponential target amplification through RT–RPA, the slope was steeper (−4.07 ± 2.40) limiting its use in quantitative RNA detection and non-communicable diseases. Furthermore, despite the sensitivity enhancement of the NLISA for preamplification-free RNA detection, we discovered that the LOD of the preamplification-based assay is determined by RT–RPA's capability to create copies of the target analyte and inclusion of the NLISA thus does not necessarily reach a lower LOD.

Given the low LOD of CrisprZyme, we next tested if the assay could be employed for the detection of different non-coding RNA (ncRNA) species since they represent promising biomarkers[18–20] but can be challenging to sense[21,22]. Indeed, CrisprZyme enabled the quantitation of synthetic standards of microRNA-223 (miR-223), aurora kinase A (AURKA) circular RNA and long non-coding RNA LIPCAR (lnc-LIPCAR) in the picomolar range (Fig. 4b). To test its correlation with an established quantitative diagnostic assay, we compared detection of miR-223 by CrisprZyme with quantitative PCR with reverse transcription (RT–qPCR) (Fig. 4c). Testing of five different samples containing miR-223 at concentrations between 20 pM and 400 pM revealed a high degree of correlation between the two assays, covering cycle threshold (C_t) values between 19 and 25 for RT–qPCR reactions.

Detection of ncRNAs in cell culture and human disease

To demonstrate the potential use of our developed assay, we applied it to sense different human ncRNAs (Fig. 5a). Since cell-type specific expression of miRNAs can serve as an indicator for cell fate conversion, we aimed to monitor in vitro differentiation from induced pluripotent stem cells (iPSCs) to cardiomyocytes through sensing of miRNA-143-3p (miR-143-3p) (Fig. 5b). CrisprZyme successfully detected upregulation of miR-143-3p in induced cardiomyocytes without preamplification, which was in agreement with previous studies[23]. To display the potential of CrisprZyme for the diagnosis of severe myocardial injury, we tested the blood of 59 patients

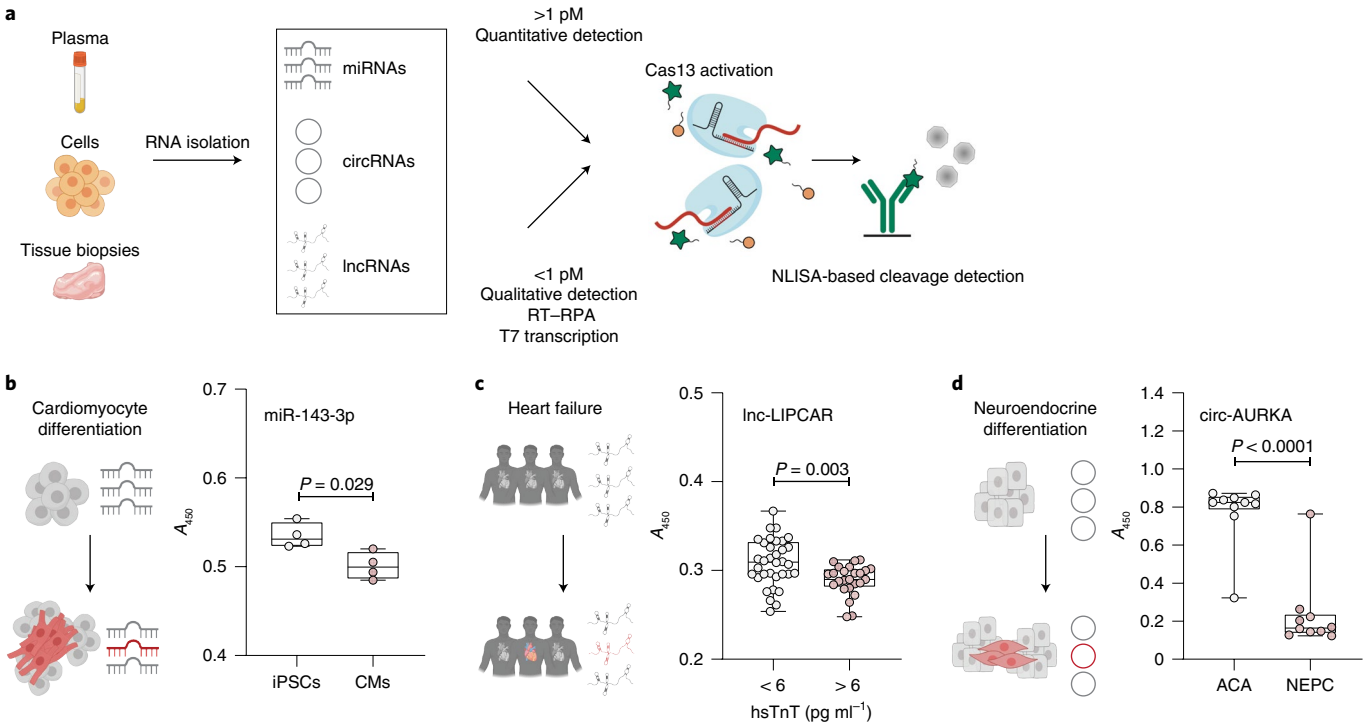

Fig. 5 | Quantification of different ncRNA species from cell culture and human plasma or tissue. a, Schematic representation of the sample analysis experimental workflow. **b**, Schematic of upregulated (red) miRNAs (grey) upon differentiation of iPSCs to cardiomyocytes (CMs) in vitro (left). Expression of miR-143-3p in iPSCs and cardiomyocytes as measured by CrisprZyme ($N = 4$ samples, $n = 2$ replicates). **c**, Schematic of upregulated (red) lncRNAs (grey) in plasma of patients with heart failure. Expression of lnc-LIPCAR in patients with heart failure and a control group as measured by CrisprZyme ($N \geq 25$ samples, $n = 2$ replicates). **d**, Schematic of upregulated (red) circRNAs (grey) in tissue biopsies from patients with prostate cancer. Expression of circ-AURKA in biopsies of ACA and NEPC as measured by CrisprZyme ($N = 10$ samples, $n = 2$ replicates). Data points represent the median of two replicates. Box and whisker plots represent median and quartiles. Mann–Whitney test.

presenting to the emergency department with chest pain for expression of lnc-LIPCAR (Fig. 5c). We observed upregulation of lnc-LIPCAR in patients with levels of high-sensitivity Troponin T (hsTnT) above 6 pg ml^{-1} as compared to a control group with levels lower than 6 pg ml^{-1}, indicating CrisprZyme's ability to identify patients with extensive myocardial infarction. Finally, circRNAs can be differentially expressed in human diseases and thereby serve as diagnostic biomarkers[24]. Thus, we aimed to differentiate two prostate cancer types: neuroendocrine prostate carcinoma (NEPC) and prostate adenocarcinoma (ACA) by measuring expression of circular AURKA RNA (circ-AURKA). This has been identified previously as a marker of NEPC[24] (Fig. 5d). Since circ-AURKA expression is very low in ACA, we aimed for a qualitative assay that detected circ-AURKA in NEPC using RT–RPA and T7 transcription for preamplification of the target region followed by its detection through CrisprZyme. To specifically sense the circular isoform, we positioned the gRNA at the back-splicing junction and used divergent RT–RPA primer for preamplification. CrisprZyme detected circ-AURKA in total RNA isolates from nine of ten NEPC biopsies, while only one of ten ACA biopsies were circ-AURKA positive.

Conclusions

We designed a nanozyme-based CRISPR-diagnostic assay, CrisprZyme, to accurately measure RNA concentration in complex samples by exploiting the high catalytic activity of Pt@Au nanozymes, which serve as signal catalysts for the cleavage of RNA reporter molecules. We functionalized the nanozymes with a biotin-binding protein and developed an NLISA that can measure reporter RNA concentrations down to femtomolar concentrations.

CrisprZyme enabled the quantification of RNA targets at room temperature with an LOD in the low picomolar range. Since CrisprZyme is independent of the gRNA design and the specific Cas enzyme, it can be widely employed to amplify CRISPR-based diagnostics that rely on the collateral cleavage of reporter oligonucleotides. The assay is also amenable to a colorimetric readout that allows for detection by the naked eye, qualitative analysis through simple imaging and quantitative analysis with a spectrometer. These results indicate the versatility of CrisprZyme in resource-limited settings, while its adaptability to 96- or 384-well plates enables testing on large scales. In addition, CrisprZyme followed by lateral-flow-based readouts facilitates the rapid analysis of samples at the point of care, while the combination with LbuCas13a allows for the quantitative preamplification-free sensing in the femtomolar range.

We showed that CrisprZyme allows the sensing of different ncRNA species including miRNAs, lncRNAs and circRNAs. We detected miRNAs indicative of cell differentiation from iPSCs to cardiomyocytes in cultured cell extracts. This presents CrisprZyme as an alternative approach to monitor cell differentiation in research laboratories. We also challenged CrisprZyme with the analysis of lnc-LIPCAR in blood from patients presenting with chest pain at hospital emergency rooms and circ-AURKA in tumour biopsies from patients with prostate cancer. Our results showed a significant difference between the patient cohorts and a clear performance capability for non-communicable diseases, indicating the diagnostic potential of CrisprZyme in complex clinical specimens.

CrisprZyme offers the possibility for the preamplification-free, quantitative detection of ncRNA species, and its combination with preamplification techniques allows for the qualitative sensing of RNA in the low femtomolar range. Future improvements of the

assay will likely include a shorter assay time as well as the fast extraction of RNA from crude clinical samples, followed by Cas-mediated cleavage and nanozyme detection on a microporous nitrocellulose membrane substrate.

Online content

Any methods, additional references, Nature Research reporting summaries, source data, extended data, supplementary information, acknowledgements, peer review information; details of author contributions and competing interests; and statements of data and code availability are available at https://doi.org/10.1038/s41565-022-01179-0.

Received: 29 July 2021; Accepted: 15 June 2022;
Published online: 4 August 2022

References

1. Pardee, K. et al. Rapid, low-cost detection of Zika virus using programmable biomolecular components. *Cell* **165**, 1255–1266 (2016).
2. Gootenberg, J. S. et al. Nucleic acid detection with CRISPR–Cas13a/C2c2. *Science* **356**, 438–442 (2017).
3. Gootenberg, J. S. et al. Multiplexed and portable nucleic acid detection platform with Cas13, Cas12a, and Csm6. *Science* **360**, 439–444 (2018).
4. Harrington, L. B. et al. CRISPR–Cas12a target binding unleashes indiscriminate single-stranded DNase activity. *Science* **360**, 436–439 (2018).
5. Lee, R. A. et al. Ultrasensitive CRISPR-based diagnostic for field-applicable detection of *Plasmodium* species in symptomatic and asymptomatic malaria. *Proc. Natl Acad. Sci. USA* **117**, 25722–25731 (2020).
6. Bruch, R. et al. CRISPR/Cas13a-powered electrochemical microfluidic biosensor for nucleic acid amplification-free miRNA diagnostics. *Adv. Mater.* **31**, 1905311 (2019).
7. Kaminski, M. M. et al. A CRISPR-based assay for the detection of opportunistic infections post-transplantation and for the monitoring of transplant rejection. *Nat. Biomed. Eng.* **4**, 601–609 (2020).
8. Li, L. et al. HOLMESv2: a CRISPR–Cas12b-assisted platform for nucleic acid detection and DNA methylation quantitation. *ACS Synth. Biol.* **8**, 2228–2237 (2019).
9. Dai, Y. et al. Exploring the trans-cleavage activity of CRISPR–Cas12a (cpf1) for the development of a universal electrochemical biosensor. *Angew. Chem. Int. Ed.* **58**, 17399–17405 (2019).
10. Li, S.-Y. et al. CRISPR–Cas12a-assisted nucleic acid detection. *Cell Discov.* **4**, 20 (2018).
11. Wong, Y.-P., Othman, S., Lau, Y.-L., Radu, S. & Chee, H.-Y. Loop-mediated isothermal amplification (LAMP): a versatile technique for detection of micro-organisms. *J. Appl. Microbiol.* **124**, 626–643 (2018).
12. Wang, D.-G., Brewster, J. D., Paul, M. & Tomasula, P. M. Two methods for increased specificity and sensitivity in loop-mediated isothermal amplification. *Molecules* **20**, 6048–6059 (2015).
13. Loynachan, C. N. et al. Platinum nanocatalyst amplification: redefining the gold standard for lateral flow immunoassays with ultrabroad dynamic range. *ACS Nano* **12**, 279–288 (2018).
14. Kellner, M. J., Koob, J. G., Gootenberg, J. S., Abudayyeh, O. O. & Zhang, F. SHERLOCK: nucleic acid detection with CRISPR nucleases. *Nat. Protoc.* **14**, 2986–3012 (2019).
15. Kaminski, M. M., Abudayyeh, O. O., Gootenberg, J. S., Zhang, F. & Collins, J. J. CRISPR-based diagnostics. *Nat. Biomed. Eng.* **5**, 643–656 (2021).
16. Abudayyeh, O. O. et al. RNA targeting with CRISPR–Cas13. *Nature* **550**, 280–284 (2017).
17. Shan, Y., Zhou, X., Huang, R. & Xing, D. High-fidelity and rapid quantification of miRNA combining crRNA programmability and CRISPR/Cas13a trans-cleavage activity. *Anal. Chem.* **91**, 5278–5285 (2019).
18. Shi, T., Gao, G. & Cao, Y. Long noncoding RNAs as novel biomarkers have a promising future in cancer diagnostics. *Dis. Markers* **2016**, 9085195 (2016).
19. Beermann, J., Piccoli, M.-T., Viereck, J. & Thum, T. Non-coding RNAs in development and disease: background, mechanisms, and therapeutic approaches. *Physiol. Rev.* **96**, 1297–1325 (2016).
20. Wang, C. & Jing, Q. Non-coding RNAs as biomarkers for acute myocardial infarction. *Acta Pharmacol. Sin.* **39**, 1110–1119 (2018).
21. Zhu, C.-S. et al. Avenues toward microRNA detection in vitro: a review of technical advances and challenges. *Comput. Struct. Biotechnol. J.* **17**, 904–916 (2019).
22. Dave, V. P. et al. MicroRNA amplification and detection technologies: opportunities and challenges for point of care diagnostics. *Lab. Invest.* **99**, 452–469 (2019).
23. Garate, X. et al. Identification of the miRNAome of early mesoderm progenitor cells and cardiomyocytes derived from human pluripotent stem cells. *Sci. Rep.* **8**, 8072 (2018).
24. Chen, S. et al. Widespread and functional RNA circularization in localized prostate cancer. *Cell* **176**, 831–843.e22 (2019).

Methods

Recombinant production of LbuCas13a from *Leptotrichia buccalis* C-1013-b. The expression vector pC0072 LbuCas13a His6-TwinStrep-SUMO-BsaI was a gift from F. Zhang (Addgene plasmid no. 115267; RRID:Addgene_115267; ref. [3]). The protein was produced using *Escherichia coli* T7 Express cells (NEB) co-transformed with the pRARE2 plasmid. TB media was supplemented with 100 μg ml^{-1} ampicillin and 34 μg ml^{-1} chloramphenicol. The cultures were grown at 37 °C until the optical density at a wavelength of 600 nm reached approximately 2.0. Gene expression was induced by the addition of 0.5 mM isopropyl β-D-1-thiogalactopyranoside at 17 °C. After induction, cultures were grown overnight at 17 °C. Cells were harvested by centrifugation and the pellets were stored at −80 °C.

For purification, cells were resuspended in lysis buffer (50 mM Tris pH 8.0, 0.5 M KCl, 5% glycerol, 1 mM $MgCl_2$), supplemented with cOmplete (EDTA-free protease inhibitor cocktail, Roche), 0.5 mM dithiothreitol (DTT), 1 mM phenylmethyl-sulfonyl fluoride and 6.000 U ml^{-1} lysozyme (Serva), and lysed by sonication (SONOPULS HD 2200, Bandelin Electronic GmbH & Co. KG). The extract was cleared by centrifugation at 36,000*g* and the His6-fusion protein was captured from the supernatant using affinity chromatography on a 5 ml Ni Sepharose 6Fast Flow column (Cytavia), equilibrated with 50 mM Tris-HCl pH 8.0, 0.5 M KCl, 5% glycerol, 1 mM $MgCl_2$ and 0.5 mM DTT. Before elution with elution buffer (20 mM Tris-HCl pH 8.0, 0.5 M KCl, 5% glycerol, 0.5 mM DTT, 0.2 M imidazole pH 8.0), the bound protein was washed three times with various wash buffers (1, 20 mM Tris-HCl pH 8.0, 1 M KCl, 5% glycerol, 0.5 mM DTT, 5 mM imidazole pH 8.0; 2, 20 mM Tris-HCl pH 8.0, 0.5 M KCl, 5% glycerol, 0.5 mM DTT, 5 mM imidazole pH 8.0; 3, 20 mM Tris-HCl pH 8.0, 0.5 M KCl, 5% glycerol, 0.5 mM DTT, 15 mM imidazole pH 8.0) to remove contaminating nucleic acids and proteins. The eluted protein was supplemented with 5% glycerol and 0.5 mM DTT, and the fusion tag was cleaved off by adding 1:75 (w/w) yeast Ulp1p SUMO protease. The protein was further purified by ion exchange chromatography on an HiTrap Heparin HP column (Cytavia), equilibrated with 20 mM Hepes-NaOH pH 7.5, 0.25 M KCl, 5% glycerol and 1 mM DTT. The purification additionally included a size-exclusion chromatography step on a 26/600 Superdex 200 prep grade column (Cytavia), equilibrated with 50 mM Tris-HCl pH 7.5, 1 M NaCl and 1 mM DTT. The storage buffer of the protein was adjusted to 50 mM Tris-HCl pH 7.5, 600 mM NaCl, 5% glycerol and 2 mM DTT. The purified protein was flash-frozen in small aliquots with liquid nitrogen and stored at −80 °C until further use.

Buffers. RNase-free ultrapure distilled water (UPDW, Invitrogen) was used in all experiments. All buffers were prepared in RNase-free conditions. Phosphate buffer saline is 0.01 M phosphate buffer in a 0.8% w/v saline solution, pH 7.5. Coating buffer is a 0.05 M carbonate-bicarbonate buffer, pH 9.6. Citrate buffer is 50 mM sodium citrate, pH 5.0. The substrate solution contains 0.01% w/v 3,3′,5,5′-tetramethylbenzidine and 0.02% v/v H_2O_2 in citrate buffer. The 10X Cleavage buffer is 200 mM HEPES, 600 mM NaCl, 90 mM $MgCl_2$, pH 6.

Pt@Au synthesis. The 188 nm Pt@Au was synthesized by further overgrowing Pt onto 120 nm Pt@Au. The 120 nm Pt@Au preparation is described elsewhere[13]. Briefly, 835 μl of UPDW, 165 μl of Pt@Au (120 nm, 500 pM), 20 μl of PVP (20% w/v, 10 kDa, Sigma), 40 μl of L-ascorbic acid (100 mg ml^{-1}, Sigma), 40 μl of $H_2PtCl_6 \times 6H_2O$ (100 mM, Sigma) was added into a 1.5 ml glass vial in this order of addition. It was vortexed and immediately incubated at 65 °C for 1 h. Pt@Au was then cooled to room temperature, and excess reagents were removed through three sequential washing cycles at 7,000*g* for 5 min with UPDW. The product was resuspended in UPDW to have a final volume of 165 μl of Pt@Au (500 pM).

Pt@Au characterization. All batches of Pt@Au were diluted to 6.25 pM in UPDW and characterized using Zetasizer nano series ZEN3600 to measure the charge and particle size based on the zeta potential and DLS, respectively. TEM imaging, STEM imaging and EDS analyses were performed on a JEOL JEM-2100F field emission electron microscope operating at 200 kV, equipped with Gatan Orius SC 1000 CCD camera (2*k*×4*k*), Gatan annular bright field, Gatan HAADF and EDS detectors (Oxford Instruments INCA EDS 80 mm X-Max detector system with STEM capability). Before the imaging and analyses, the samples were prepared by placing a 2 μl droplet of the nanoparticle dispersion on a 200-mesh carbon-coated copper grid (Electron Microscopy Science, USA). AZtecTEM Software (Oxford Instruments) was used for all EDS data acquisition and processing and TruMap mode in AZtecTEM was used for the elemental mapping.

Pt@Au functionalization. Pt@Au was functionalized with streptavidin or neutravidin by mixing 200 μl Pt@Au (500 pM), 20 μl phosphate buffer (50 mM, pH 6.4) and 20 μl of biotin-binding protein (1 mg ml^{-1}). The mixture was shaken at 700 r.p.m. for 3 h at room temperature. Then 100 μl of blocking protein (beta casein or BSA at 1 mg ml^{-1}) or PBST was added into the mixture. It was then shaken at 700 r.p.m. for 1 h at room temperature. The excess reagents were removed through three sequential washing cycles at 7,000*g* for 5 min with PBST. The product was resuspended in PBST to have a final volume of 200 μl of streptavidin-Pt@Au or neutravidin-Pt@Au (500 pM).

NLISA. A microtitre plate (384 wells, Maxisorp, Nunc) was coated with anti-FAM antibody (100 ng ml^{-1} in coating buffer, 40 μl per well, Abcam) for 3 h at room temperature and covered with an adhesive plate sealer. The plate was washed three times with PBST (100 μl per well), and 28 μl of PBST was added per well followed by the solution containing the reporter RNA (5′-FAM-UUUUUC-biotin-3′, from 10 nM to 10 fM and 0 in PBST, 14 μl per well) or the LwaCas13a reaction mixture (14 μl per well). After 30 min at room temperature, the plate was washed as before, and a solution of streptavidin-Pt@Au (0.5 pM in PBST, 40 μl per well) was added to the wells and incubated for 30 min at room temperature. The plate was washed again, and the substrate solution was added (40 μl per well). Colour development was stopped after 30 min at room temperature with 4N H_2SO_4 (20 μl per well). Signal readout was plotted based on absorbance at 450 nm (Spectramax M5, Molecular Devices) or central pixel blue intensity of each well measured using image software (FIJI on Surface Pro 4) of a photo of the plate (Samsung Galaxy Note 10 plus, 16 MP rear camera).

Target RNA. Synthetic target RNA was supplied by Integrated DNA Technologies. The RNA used in this study is summarized in Supplementary Table 3. RT–RPA primers were complementary to the RNA target sequence. They were designed such that the forward primer was at the 5′ end of the target site that is bound by the gRNA's spacer, while the reverse primer was at the 3′ end. The forward primers also contain a T7 promoter sequence, enabling DNA amplicons to be first transcribed to RNA before Cas13-based detection. The primers were ordered as DNA (Supplementary Table 4, Biomers).

gRNA production. LwaCas13a and LbuCas13a gRNAs, respectively, contained 28 and 20 nucleotide-long spacers complementary to the target site. For miRNA targets, spacers were designed to include the entire miRNA length. Constructs were ordered as DNA (Supplementary Table 5, Biomers/ Eurofins) with an appended T7 promoter sequence for in vitro RNA transcription. Synthesis of gRNAs was performed using the HiScribe T7 Quick High Yield RNA Synthesis kit (New England Biolabs) according to the manufacturer's instructions and purified using the Monarch RNA Cleanup Kit (50 μg, New England Biolabs). DNA oligonucleotides containing a T7 promoter sequence served as templates. gRNA purity was checked using Bioanalyzer (Agilent) Small RNA Analysis Kit following the supplier's protocol.

CRISPR reaction. A Master Mix was prepared with a concentration of 3× of Cleavage buffer, 1.5 U μl^{-1} Murine RNase Buffer (New England Biolabs), 375 nM of RNase Alert V2 (Thermo Fisher Scientific), 135 nM of LwaCas13a (Genscript) and 67.5 nM gRNA. Then 10 μl of synthetic RNA standards (from 1 μM to 10 pM and 0 pM, prepared in 10 ng μl^{-1} of PolyA RNA carrier) or samples were mixed with 5 μl of LwaCas13 reaction Master Mix in a 384-well black clear-bottom plate (Corning) and left to react for 3 h at 25 or 37 °C. Fluorescence was measured at 490/520 nm every 5 min for 3 h (Spectramax M5, Molecular Devices).

When combined with NLISA (CrisprZyme), the Master Mix was prepared with a concentration of 3× of Cleavage buffer, containing 1.5 U μl^{-1} Murine RNase Buffer (New England Biolabs), 0.75 nM of 5′-FAM-UUUUUC-Biotin-3′ (Integrated DNA Technologies), 300 nM of LwaCas13a (GeneScript) and 360 nM gRNA. Then 10 μl of synthetic RNA standards (from 2,000 pM to 0.5 pM and 0 pM, prepared in 10 ng μl of PolyA carrier) or samples were mixed with 5 μl of LwaCas13 reaction Master Mix in a 384-well PCR plate (Thermo Fisher Scientific) and left to react for 3 h at room temperature. Then 14 μl were provided as input for the NLISA. Reactions with LbuCas13a were performed similarly, with final concentrations of 10 mM Tris-HCl buffer, 10 mM NaCl, 1.5 mM $MgCl_2$, 1 U μl^{-1} Murine RNAse Buffer (New England Biolabs), 1.25 ng μl^{-1} HEK293T RNA, 0.1 nM of 5′-FAM-UUUUUC-Biotin-3′ (Integrated DNA Technologies), 100 nM of LbuCas13a and 65.5 nM gRNA.

LFA. The lateral flow strips with anti-FAM test line were produced using an automated liquid dispenser (BioDot System AD3220). Here 0.5 mg ml^{-1} of filtered (0.2 μM filter) anti-FAM antibody (Abcam 19224, lot GR175456-62) was dispensed at a height of 5 mm from the bottom of the nitrocellulose (CN95 Unisart Nitrocellulose Membrane, Sartorius) before being dried overnight at 37 °C. Lateral flow half-dipstick assays were then assembled onto backing card (Kenosha, KN-PS1060.19) with overlapping absorbent pad material (Ahlstrom-munksjo, KN-222-20.1), before being cut into 4-mm-wide test strips.

The LFAs were run in half-dipstick format by dipping the test strips into a 96-well plate (Corning no. 3641, flat bottom, non-binding surface) containing 10 μl of Cas reaction product, 50 μl PBST, 10 μl of streptavidin-functionalized Pt@Au (1 pM, blocked with beta casein). After the solution had fully wicked up the strip (around 10 min), the strip was then dipped in another well containing 100 μl of PBST for 10 min to wash through any unbound nanoparticles or reporter RNA. Subsequently, the strip was submerged in another well for 10 min filled with 330 μl (enough solution to cover the test line on the strip in the well) freshly prepared PtNC substrate solution containing 38% 1× Pierce CN/DAB (4-chloro-1-naphthol/3,3′-diaminobenzidine, tetrahydrochloride) Substrate Kit (Thermo Scientific), 12% (w/w) hydrogen peroxide (Sigma) and 50% (v/v) stable peroxide buffer. Finally, the strip was moved into a well containing 330 μl purified water

for up to 10 min to stop the reaction and it was then briefly dried under ambient conditions for ease of handling. Strips were imaged with an iPhone XS mobile phone camera. Test line intensities were quantified using ImageJ by first converting the image to grayscale (32 bit) before drawing a rectangle the width of the lateral flow strips and length long enough to include an internal control of one of the background grid lines. Using the gel analyser tool, the pixel density of each test line was integrated before being normalized relative to the pixel density of the internal control.

RT–RPA. RT–RPA was performed using the TwistAmp Basic Kit (TwistDx) as per the manufacturer's instructions and with the following modifications. The total reaction volume was 20 µl. First, 3.08 µl of RNA target and 1.92 µl of a 10 µM 1:1 mix of forward and reverse primers were heated for 10 min at 65 °C. A master mix was then prepared for the resuspension of TwistAmp Basic reaction pellets, where each pellet was resuspended with 29.5 µl rehydration buffer, 2.05 µl UPDW, 0.95 µl DTT (Sigma-Aldrich) at 1 M, 2.5 µl GoScript reverse transcriptase (Promega) at 160 U µl^{-1} and 2.5 µl MgOAc at 280 mM. Then 15 µl of the resuspended TwistAmp Basic reactions was added to each 5 µl RNA target–primer mixture, resulting in forward and reverse primers at 480 nM, DTT at 19 mM and GoScript reverse transcriptase at 8 U µl^{-1}. Each reaction was incubated at 42 °C for 60 min.

RT–qPCR. miScript II RT Kit (Qiagen) was used for reverse transcription and miScript SYBR Green PCR Kit (Qiagen, miScript Primer Assay MS00003871) for qPCR following the supplier's protocol. Reverse transcription was performed with 10 µl of input, synthetic RNA standards (from 1,000 to 0.1 fM and non-targeting control, prepared in 1 ng µl^{-1} of PolyA carrier) or samples in 0.2 ml PCR tubes. qPCR was performed with 1 µl as input in a 384-well PCR plate on a QuantStudio 6 cycler (Thermo Fisher). Samples were interpolated using standard regression, and samples with a concentration of miR-223 > 1 pM were selected and analysed by CrisprZyme.

Cell culture and cell differentiation. The human episomal iPSC line (Thermo Fisher) was maintained in the complete Essential 8 medium (Thermo Fisher) on 6-well plates coated with Matrigel (Corning) diluted in DMEM/F12 (Thermo Fisher). The cells were regularly split at a 1:12 ratio every 4 days using 0.5 mM EDTA. The medium was supplemented with 10 µM Rock inhibitor Y-27632 (STEMCELL Technologies) for the first 24 h after passaging to avoid cell dissociation-induced apoptosis. Cardiac differentiation was optimized from the previously reported protocol[25] as follows: the iPSC medium was changed to the differentiation medium, RPMI supplemented with 2% v/v B27-insulin supplement (Thermo Fisher), 4 days after the split, when cells reached ~85% confluence. From day 0 to day 2, the differentiation medium was supplemented with 6 µM CHIR99021 (tebu-bio) and replaced with the fresh differentiation medium on day 2. From day 3 to day 5, the differentiation medium supplemented with 2.5 µM Wnt-C59 (Stratech) was applied. On day 5, the medium was replaced with the fresh differentiation medium. The medium was switched to RPMI supplemented with 2% v/v B27 supplement (Thermo Fisher) on day 7 and replaced with fresh medium every other day. Spontaneous contraction of the cells was observed from day 7. The medium was switched to the RPMI without glucose supplemented with 2% v/v B27 supplement (Thermo Fisher) and 5 mM sodium lactate (Merck), and changed every other day for the metabolic selection of cardiomyocytes from day 11 to day 17. ncRNA was extracted on day 17 following the protocol described below.

Patient cohort. Plasma samples for the evaluation of lnc-LIPCAR were obtained from discarded material from clinical samples initially obtained from adults (>18 years) presenting to Massachusetts General Hospital with chest pain and tested for hsTnT. The material was excess to clinical needs and selected based on hsTnT values and the fact that it was stored at 4 °C for <12 h after initial blood draw. Plasma was then frozen at −80 °C before research use. The study was granted exemption from informed consent due to the use of anonymized discarded clinical samples and was approved by the Mass General Brigham IRB, Protocol no. 2019P002499.

RNA specimens extracted from tissue biopsies for the measurement of circ-AURKA were obtained through the Prostate Cancer Biorepository Network (PCBN), a US Department of Defense/Congressionally Directed Medical Research Program bioresource. All samples were de-identified (MIT exempt determination E-1564). Primary adenocarcinoma samples were provided by Johns Hopkins University and neuroendocrine castration-resistant prostate cancer samples were provided by the University of Washington through RNA extraction of metastatic cancer tissue.

ncRNA extraction from samples. ncRNA was extracted from a cell pellet or 200 µl of blood using the miRNeasy Micro Kit (Qiagen) following the supplier's protocol. Then 3.5 µl of the Spike-In Control (Ce-miR-39, 1.6 ×10^8 copies µl^{-1}) was added after the QIAzol Reagent. ncRNAs were eluted from the RNeasyMinElute spin column with two washes of 14 µl and 8 µl of UPDW (total RNA > 30 ng µl^{-1}, $A_{260/280}$ > 1). ncRNAs were diluted to 2.5 ng µl^{-1} of total RNA to be used as input for RT–RPA (3.08 µl) and LwaCas13a reaction (10 µl).

Data and statistical analysis. All data analysis was conducted in GraphPad v.9.0.0 (Prism). All the sample sizes and statistical tests are specified in the figure legends. Calibration curves were fitted to a four-parameter equation according to Supplementary equation 1, where maximum signal and minimum signal are plateaus in the units of the absorbance, EC50 is the concentration producing 50% of the maximal signal and Hillslope is the slope at the inflection point of the sigmoid curve. LOD was defined as the 10% signal of the maximum signal. Results were normalized defining 0% as the smallest mean in each dataset and 100% as the largest mean in each dataset.

Data availability

Research data are available online at https://doi.org/10.5281/zenodo.6553774.

References

25. Burridge, P. W. et al. Chemically defined generation of human cardiomyocytes. *Nat. Methods* **11**, 855–860 (2014).

Acknowledgements

We acknowledge use of the characterization facilities at the Harvey Flower Electron Microscopy Suite (Department of Materials, Imperial College London). We thank the PCBN for providing patient samples. This work was supported by the Department of Defense Prostate Cancer Research Program, US Department of Defense Award Nos W81XWH-18-2-0013, W81XWH-18-2-0015, W81XWH-18-2-0016, W81XWH-18-2-0017, W81XWH-18-2-0018 and W81XWH-18-2-0019 PCRP PCBN. M.B. and M.M.S. acknowledge funding from the British Heart Foundation (grant no. RE/18/4/34215) and the EPSRC IRC in Early Warning Sensing Systems for Infectious Diseases (i-sense) Mobility Fund (grant no. EP/K031953/1). M.M.K. was supported by the German Academy of Sciences, Leopoldina (grant no. LPDS 2018-01) and the Emmy Noether Programme (grant no. KA5060/1-1). M.M.K. is a participant in the BIH Charité Clinician Scientist Program funded by the Charité – Universitätsmedizin Berlin and the Berlin Institute of Health at Charité (BIH). C.A. was supported by the Singapore A*STAR National Science Scholarship fellowship. A.J.S. was supported by the MD Research Stipend of the BIH. H.K. and M.M.S. acknowledge funding from the Research Council of Norway through its Centres of Excellence scheme (grant no. 262613). X.T. is supported by an American Gastroenterological Association Takeda Pharmaceuticals Research Scholar Award in Inflammatory Bowel Disease and the Wyss Institute. J.J.C. was supported by the Paul G. Allen Frontiers Group and the Wyss Institute. M.M.S. acknowledges funding from the EPSRC IRC in Agile Early Warning Sensing Systems for Infectious Diseases and Antimicrobial Resistance (i-sense2) (grant no. EP/R00529X/1), the Royal Academy of Engineering Chair in Emerging Technologies award (no. CiET2021\94) and the Rosetrees Trust. We thank A. Schütz and the team of the Protein Production & Characterization Technology Platform of the Max Delbrück Center for Molecular Medicine in the Helmholtz Association (MDC), Berlin, Germany (https://www.mdc-berlin.de/protein-production-characterization) for producing the LbuCas13a protein.

Author contributions

M.B., M.M.K., J.J.C. and M.M.S. conceived and designed the research. M.B., M.M.K. and C.A. carried out all the experiments and analysed the data. N.K. performed the LFA experiments, TEM, STEM and EDX imaging and analyses. R.G. and A.J.S. performed RT–RPA, assisted in the design and production of gRNAs and in the optimization of LbuCas13a detection. S.D.-P. optimized and printed LFA strips. X.T. and A.S.D. collected patient samples and edited the manuscript. H.K. performed cell differentiation. M.B., M.M.K., J.J.C. and M.M.S. wrote the manuscript with feedback from all the authors.

Competing interests

M.M.S., M.B., C.A. and S.D.-P. have filed a patent application (2110729.7) covering the techniques and assay design as described in the manuscript. J.J.C. is a co-founder and director of Sherlock Biosciences. The other authors declare no competing interests.

Additional information

Supplementary information The online version contains supplementary material available at https://doi.org/10.1038/s41565-022-01179-0.

Correspondence and requests for materials should be addressed to James J. Collins or Molly M. Stevens.

Peer review information *Nature Nanotechnology* thanks the anonymous reviewers for their contribution to the peer review of this work.

Reprints and permissions information is available at www.nature.com/reprints.